IV Simpósio Paranaense de Modelagem, Simulação e Controle de Processos
ISSN : 1984-7521
Artigo: 04
Páginas: 25 - 31

NUMERICAL ANALYSIS OF NUCLEATE BOILING FLOW IN A PILOT-SCALE THERMOSIPHON

Bruna Iten Bittelbrunn[1]*, Roberto Fischer Jr. [1], Harlley Henrique Parno[1], Henry França Meier[1], Jaci Carlo Schramm Câmara Bastos[1]

1 – University of Blumenau – FURB, Blumenau - SC, brunaiten@gmail.com

Abstract

Thermosiphons, or natural circulation loops, are circuits in which a flow pattern is driven by buoyancy forces originated from density differences, a consequence of temperature gradient. In this study, an evaporation section was evaluated by numerical simulations, in order to determine heat flux conditions for a pilot-scale thermosiphon. A two-fluid Eulerian-Eulerian model was used to represent multiphase fluid dynamic, including heat transfer and phase change effects. The results showed that a 1000 W rate is enough to generate a nucleate boiling regime. Rates up to 2000 W produce a mean vapor volume fraction greater than 0.30 at boiling region. As a result, the pilot-scale thermosiphon was designed with four 500 W electrical resistances.

Keywords: Pilot-scale thermosiphon. Nucleate boiling. CFD.

Introduction

Thermosiphons are heat transfer systems which operate based on the principle of natural circulation, generating single-phase and multiphase regimes [1]. In the first condition, the fluid temperature rises due to the heat given to the system. This temperature gradient results in a density difference, which is the driving force to the natural circulation phenomenon. In the second condition, the heat given to the system is enough to evaporate the fluid, which generates a multiphase turbulent regime with heat and mass transfer [2]. These systems are widely used in industrial applications due to relatively simple project and working principles, along with the capacity of a high heat transfer rate [3]. In a thermosiphon, heat is added to the system at the evaporation section and vapor is formed from a liquid pool. Vapor rises through the adiabatic section heading to the condenser, where it condensates releasing latent heat. The condensate returns to the evaporator as a result of the natural circulation effect ruling the system [4].

Computational fluid dynamics (CFD) became a valuable tool to predict and comprehend the behavior of thermosiphon systems. Experimental and numerical investigations are commonly performed to determine characteristics of the system and the effect of numerous parameters on equipment performance [4-6]. However, despite the constant development of models and methods, a joint analysis of a numerical approach and physical experiments is still needed in order to verify and validate numerical solutions. In this context, the aim of this paper is to project an evaporation section of a pilot-scale thermosiphon operating with constant heat flux. Therein, the section was analyzed via numerical simulation with the RPI model for wall heat flux.

Experimental

The experimental unit consists in a loop with an evaporation section and a condensation section. Fig. 1 shows the tridimensional project of the experimental unit. The evaporation section was set to be designed to operate with constant heat flux regime. Therefore, it was divided in two subsections: a 0.5 m high heated subsection (a), containing a boiler tube ASTM A213 with 40.2 mm internal diameter; and a 0.8 m high glass visualization subsection (b). The liquid-vapor separator (d) consisted in a cylindrical steel reservoir with 200 mm internal diameter and 300 mm length, adding up to a volume of 10 L, destinated to allow only vapor to enter the condenser (c). The condenser returned the vapor to the system while avoiding pressure peaks due to its atmospheric operational conditions. Once condensed, working fluid flowed to the downcomer (e), which is made of glass and kept at constant temperature.

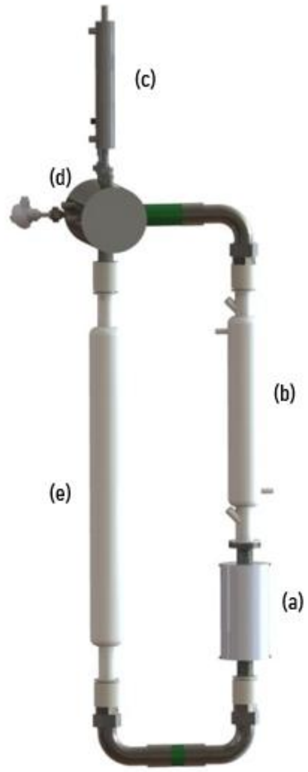

Figure 1 – Thermosiphon unit project.

In order to quantify the power needed to generate the multiphase regime on the heating section, a numerical analysis was conducted on the evaporation section. The studied section consisted in a 1.3 m high tube with a 40.2 mm internal diameter. From the total length, a 0.3 m section was heated by a constant heat flux. A two-fluid Eulerian-Eulerian approach was adopted to describe the flow. Due to phase changes, conservation equations showed in Eq. 1 to 6 were used along with RPI wall boiling model based on the partitioned heat flux hypothesis, as shown in Eq. 7 to 9 [7]. The RPI model was used to describe the wall heat flux with Kocamustafaogullari and Ishii correlation for bubble departure diameter [8], Hibiki and Ishii model for active nucleation sites density [9], and Cole equation for bubble departure frequency [10], showed in Eq. 10 to 14. Turbulence was modelled by the k-omega SST model [11] presented in Eq. 15 and 16. The phases were related according to the Tomiyama et al. drag model [12] indicated in Eq. 17. The mathematical modeling is shown in Table 1. The grid had 33,075 elements. Transient simulations were conducted with a time step of 10^{-4} s and a residual convergence criterion of 10^{-4}.

At the boiling region, a constant heat flux condition was imposed. The heat fluxes were proportional to 1000 W and 2000 W rates. Other parts of the analyzed section were considered as adiabatic regions, since they will be insulated at the pilot-scale unit. Pressure boundary condition was imposed at both inlet and outlet. All stages of the simulation were conducted in ANSYS® commercial software. Analysis were made at three distinct heights, in order to evaluate flow behavior before and after the boiling section.

Table 1
Two-fluid Eulerian-Eulerian model.

Mass conservation equations	
Liquid phase: $\frac{\partial}{\partial t}(f_l\rho_l) + \boldsymbol{\nabla}\cdot(f_l\rho_l\mathbf{v}_l) = M_{lg}^{+} - M_{gl}^{+}$	(1)
Gas phase: $\frac{\partial}{\partial t}(f_g\rho_g) + \boldsymbol{\nabla}\cdot(f_g\rho_g\mathbf{v}_g) = M_{gl}^{+} - M_{lg}^{+}$	(2)
Momentum conservation equations	
Liquid phase: $\frac{\partial}{\partial t}(f_l\rho_l\mathbf{v}_l) + \boldsymbol{\nabla}\cdot(f_l\rho_l\mathbf{v}_l\mathbf{v}_l) = -f_l\boldsymbol{\nabla}P - \boldsymbol{\nabla}\cdot\left[f_k\left(\boldsymbol{\tau}_l - \boldsymbol{\tau}_l^T\right)\right] + M_{lg}^{+}\mathbf{v}_g - M_{gl}^{+}\mathbf{v}_l + \mathbf{F}_{lg} + (f_l\rho_l\mathbf{g})$	(3)
Gas phase: $\frac{\partial}{\partial t}(f_g\rho_g\mathbf{v}_g) + \boldsymbol{\nabla}\cdot(f_g\rho_g\mathbf{v}_g\mathbf{v}_g) = -f_g\boldsymbol{\nabla}P - \boldsymbol{\nabla}\cdot f_g\boldsymbol{\tau}_g + M_{gl}^{+}\mathbf{v}_l - M_{lg}^{+}\mathbf{v}_g + \mathbf{F}_{gl} + (f_g\rho_g\mathbf{g})$	(4)
Energy conservation equations	
Liquid phase: $\frac{\partial}{\partial t}(f_l\rho_l h_l) + \boldsymbol{\nabla}\cdot(f_l\rho_l\mathbf{v}_l h_l) = \boldsymbol{\nabla}\cdot\left(f_l\lambda_l^{ef}\boldsymbol{\nabla}T_l\right) + Q_l^{lg} + M_{lg}^{+}h_{gs} - M_{gl}^{+}h_{ls}$	(5)
Gas phase: $\frac{\partial}{\partial t}(f_g\rho_g h_g) + \boldsymbol{\nabla}\cdot(f_g\rho_g\mathbf{v}_g h_g) = \boldsymbol{\nabla}\cdot\left(f_g\lambda_g\boldsymbol{\nabla}T_g\right) + Q_g^{lg} + M_{gl}^{+}h_{ls} - M_{lg}^{+}h_{gs}$	(6)
RPI model	
Convective heat flux: $q_C'' = h_C\,(T_W - T_L)(1 - A_b)$	(7)
Evaporative heat flux: $q_E'' = V_d N_A \rho_g h_{fg} f_B$	(8)
Quenching heat flux: $q_Q'' = \frac{2\sqrt{k_l\rho_l C_{p,l} f_B}}{\sqrt{\pi}}(T_W - T_L)$	(9)
Bubble departure diameter: $d_w = 2.64\cdot 10^{-5}\left(\frac{\rho_l-\rho_g}{\rho_g}\right)^{\frac{9}{10}}\varphi\left[\frac{\sigma}{g(\rho_l-\rho_g)}\right]^{\frac{1}{2}}$	(10)
Active nucleation sites density: $N_a = N_{a1}\left[1 - \exp\left(\frac{-\varphi^2}{8\varphi_1^2}\right)\right]\left\{\exp\left[f(\rho')\frac{\lambda''}{R_C}\right] - 1\right\}$	(11)
$R_C = \frac{2\sigma[1+(\rho_l/\rho_g)]/P}{\exp\{h_{lg}(T_g - T_{sat})/(RT_gT_{sat})\}-1}$;	(12)
$f(\rho') = -0.01064 + 0.4824\rho' - 0.22712(\rho')^2 + 0.05468(\rho')^3$; $\rho' = \log\left(\frac{\rho_l-\rho_g}{\rho_g}\right)$	(13)
Bubble departure frequency: $f_B = \sqrt{\frac{4g(\rho_l-\rho_v)}{3\rho_l d_w}}$	(14)
k-omega SST model	
Turbulent kinetic energy:	
$\frac{\partial}{\partial t}(\rho k) + \boldsymbol{\nabla}\cdot(\rho\mathbf{v}k) = \boldsymbol{\nabla}\cdot\left(\left(\mu + \frac{\mu_t}{\sigma_k}\right) + \nabla k\right) + P_k - \beta^*\rho k\omega$	(15)
Turbulent energy dissipation:	
$\frac{\partial}{\partial t}(\rho\omega) + \boldsymbol{\nabla}\cdot(\rho\mathbf{v}\omega) = \boldsymbol{\nabla}\cdot\left(\left(\mu + \frac{\mu_t}{\sigma_\omega}\right) + \nabla\omega\right) + C_\alpha\frac{\omega}{k}P_k - C_\beta\rho\omega^2 + 2(1-F_1)\sigma_{\omega 2}\frac{\rho}{\omega}\nabla k\cdot\nabla\omega$	(16)
Parameters of the model:	
$C_\alpha = 5/9$; $C_\beta = 0.075$; $\beta^* = 0.09$; $\sigma_{k1} = 2$; $\sigma_{\omega 1} = 2$; $\sigma_{\omega 2} = 1.186$	
Drag model	
$F_{lg}^{drag} = \frac{3}{4d_b}C_D\rho_l f_g\left|\mathbf{v}_g - \mathbf{v}_l\right|\left(\mathbf{v}_g - \mathbf{v}_l\right)$	(17)

Results and Discussion

Fig. 2 and Fig. 3 present the vapor volumetric fraction profile for a 1000 W rate and a 2000 W rate, respectively, at three different heights: beginning (A) and end (B) of the boiling region, and at 200 mm above the end (C).

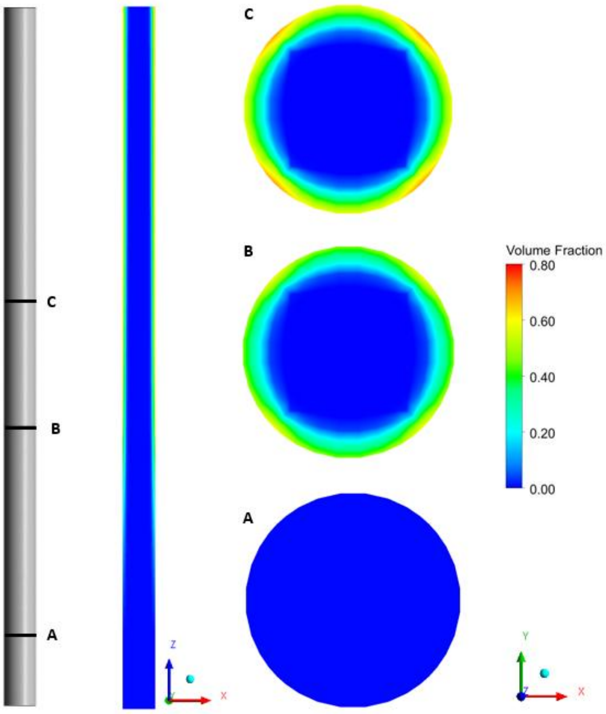

Figure 2 – Vapor volumetric fraction profile for a 1000 W rate at (A) the beginning and (B) the end of boiling section and (C) 200 mm above the end of the boiling section.

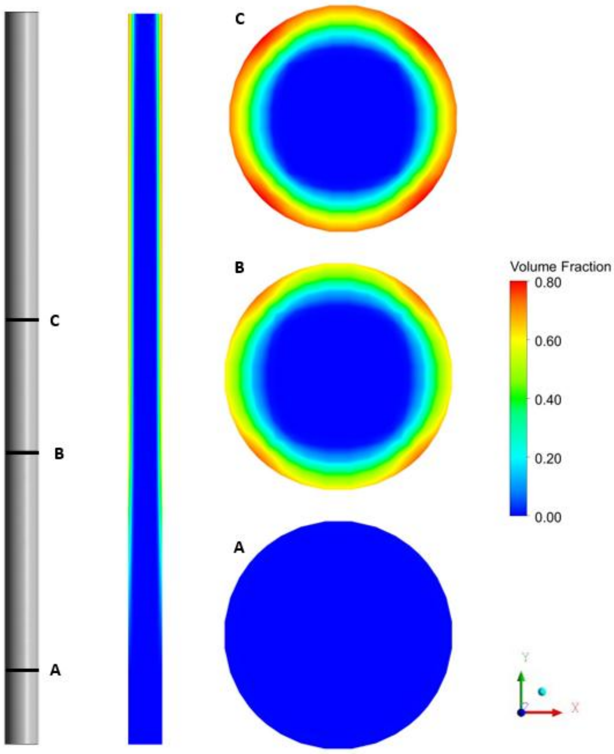

Figure 3 – Vapor volumetric fraction profile for a 2000 W rate at (A) the beginning and (B) the end of boiling section and (C) 200 mm above the end of the boiling section.

As shown in Fig. 2 and 3, vapor was formed at the delimited region where the heat flux was imposed. It was maintained near the wall and was gradually distributed on transversal section. As the boiling region ended, vapor was maintained near the wall surface and well distributed along the riser transversal section. The mean volumetric fraction at the heating area was 0.2132 for the lower heat flux and 0.3189 for the higher heat flux.

The mean temperature fields for liquid phase are shown in Fig. 4 and Fig. 5. It can be noted that the temperature near wall was significantly higher than water saturation temperature.

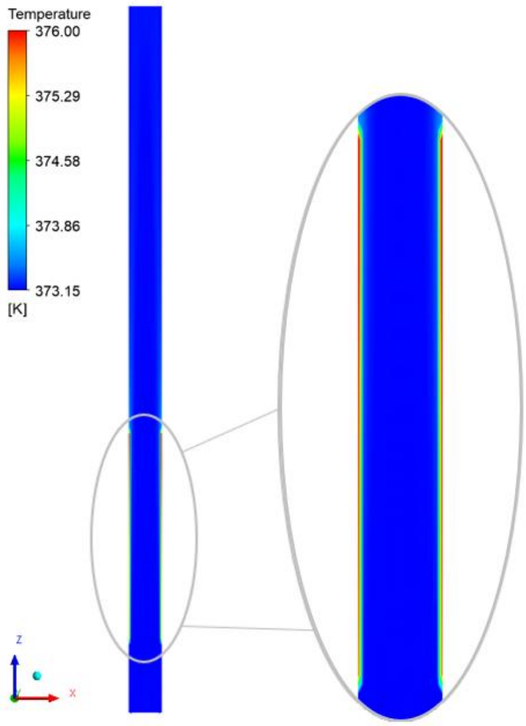

Figure 4 – Mean temperature profile at boiling section for 1000 W heat rate.

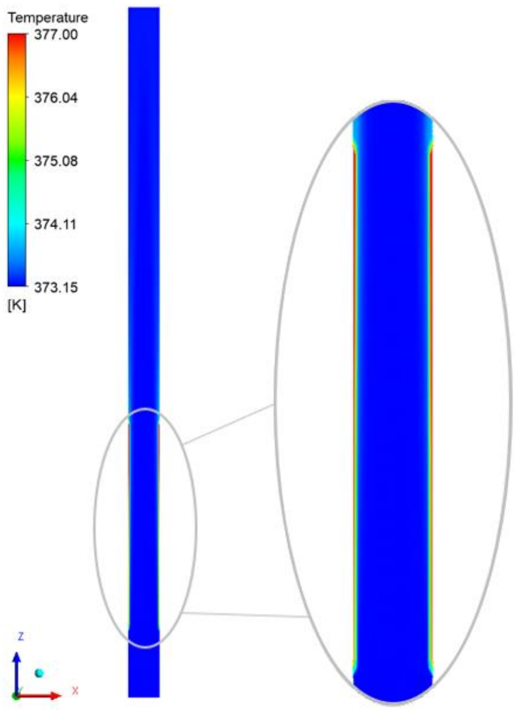

Figure 5 – Mean temperature profile at boiling section for 2000 W heat rate.

Both heat fluxes imposed to the boiling section caused the fluid to superheat near wall. For the lower heat rate, the maximum temperature reached was 378.02 K. As the heat flux was raised, temperature reached a maximum of 382.23 K at the end of heating region. This superheat might have influenced on bubble formation at adiabatic section, as observed in Fig. 2 and 3 for section C.

Conclusion

In order to generate a multiphase flow in a thermosiphon facility, a configuration was proposed based on the delimitation of a boiling section. Constant heat flux was imposed at this section. With the aim of quantifying the heat flux needed to produce vapor, numerical simulations were conducted.

The results obtained via numerical simulation indicated that the configuration was able to produce a multiphase flow. Thermal charges up to 2000 W generated a mean volumetric fraction of 0.3189 at the boiling area. As a result, the pilot-scale thermosiphon facility was designed with four 500 W electrical resistances, summing up to a 2000 W maximum rate to guarantee a large range of operational conditions. Further research will be developed at this pilot-scale unit by collecting experimental data in order to validate the proposed numerical modeling.

Acknowledgements

The authors are grateful for the financial support of PETROBRAS for this research project, through the cooperation agreement number 5850.0103010.16.9, and CNPq through Process 308714/2016-4.

References

[1] P. Zhang; B. Wang; W. Shi; X. Li. Experimental investigation on two-phase thermosyphon loop with partially liquid-filled downcomer. Applied Energy. 2015, 160, 10-17.

[2] H.R.B. Orlande, Ph.D. Thesis, Federal University of Rio de Janeiro, 1989.

[3] A. Franco; S. Filippeschi. Closed loop two-phase thermosyphon of small dimensions: A review of the experimental results. Microgravity Sci. Technol. 2012, 24, 165-179.

[4] A. Alizadehdakhel, M. Rahimi, A.A. Alsairafi. CFD modelling of flow and heat transfer in a thermosyphon. International Communications in Heat and Mass Transfer. 2010, 37, 312-318.

[5] T. Frank; P. Beckstein; C. Lifante; Burns, A.D. Prediction of subcooled wall boiling in a heated annulus including conjugate heat transfer in the central heated rod, in: Proceedings of 7th International Conference on Multiphase Flow, Tampa, 2010.

[6] E. Krepper; R. Rzehak. CFD for subcooled flow boiling: Simulation of DEBORA experiments. Nuclear Engineering and Design. 2011, 241, 3851-3866.

[7] N. Kurul; M.Z. Podowski. Multidimensional effects in forced convection subcooled boiling, in: Proceedings of 9th International Heat Transfer Conference, Jerusalem, 1990.

[8] G. Kocamustafaogullari; M. Ishii. Interfacial area and nucleation site density in boiling systems. International Journal of Heat and Mass Transfer. 1983, 26, 1377-1387.

[9] T. Hibiki; M. Ishii. Active nucleation site density in boiling systems. International Journal of Heat and Mass Transfer. 2009, 46, 2587-2601.

[10] R. Cole. A photographic study of pool boiling in the region on critical heat flux. AIChE Journal. 1960, 6,0533-542.

[11] H.P. Guerra. Masters Dissertation, University of Blumenau, 2017.

[12] A. Tomiyama; K. Isao; Z. Iztok; S. Tadashi. Drag coefficients of single bubbles under normal and micro gravity conditions. JSME International Journal. 1998, 41, 472-479.